


FULL PAPER

Open Access



# Extraordinary quasi-16-day wave activity from October 2013 to January 2014 with radar observations at mid-latitudes and MERRA2 reanalysis data

Xiansi Huang<sup>1,2</sup>, Kaiming Huang<sup>1,2,3\*</sup> , Shaodong Zhang<sup>1,2</sup>, Chunming Huang<sup>1,2</sup>, Yun Gong<sup>1,2</sup> and Hao Cheng<sup>1,2</sup>

## Abstract

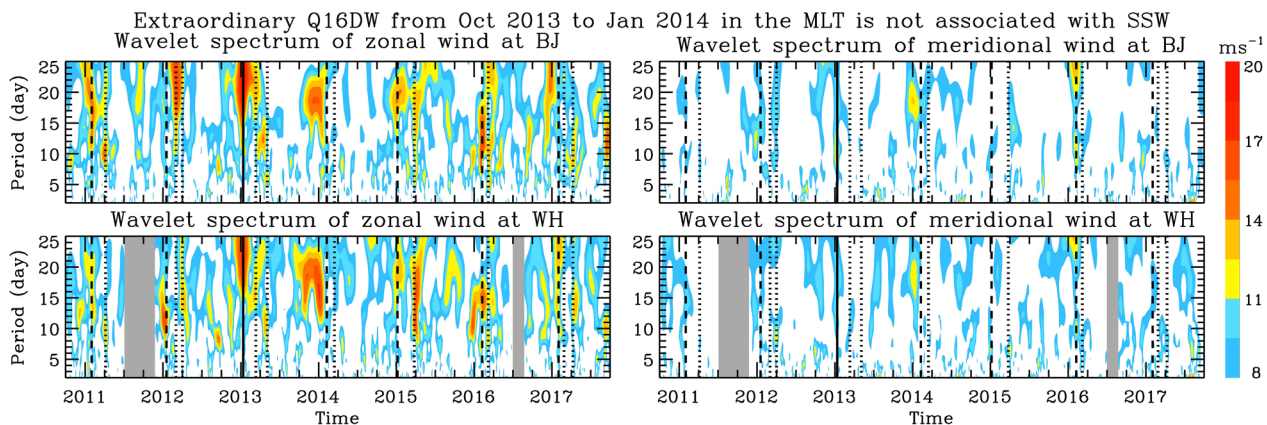
Combining two meteor radar observations at mid-latitudes and MERRA2 reanalysis data, we report an extraordinary quasi-16-day wave (Q16DW) activity in the mesosphere and lower thermosphere (MLT) from about October 2013 to January 2014. The Q16DW is not only active for a long period, but also unrelated to stratospheric sudden warming (SSW), while 7-year radar observations indicate that strong waves and oscillations in the MLT at mid-latitudes occur generally in winter, and are almost always associated with SSW and stratospheric final warming (SFW), except the extraordinary Q16DW. Meanwhile, during the SSW and SFW in February and March 2014, the observation and reanalysis data show that an intense Q16DW arises in the stratosphere but is not present in the MLT. The two Q16DWs are obviously distinguished from each other. The exceptional Q16DW shows a slowly downward phase progression from the MLT to the troposphere with predominant wavenumber 1, while the second Q16DW has a steeper vertical phase in the stratosphere with predominant wavenumber 2. Although the eastward winds prevail, these Q16DWs are weakened and evanescent in the region with the westward wind and negative refractive index. EP flux vector indicates that these waves originate mainly from the lower atmosphere at mid- and high-latitudes, and are intensified in the middle stratosphere. The first Q16DW may make a little contribution to polar vortex intensification due to small EP flux divergence. However, the Q16DW in the SSW has a strong negative divergence almost in the whole polar stratosphere, implying an important role in the stratospheric zonal wind reduction in the SSW.

**Keywords:** Q16DW, SSW, EP flux, Refractive index, MERRA2 data

\*Correspondence: hkm@whu.edu.cn

<sup>3</sup> State Observatory for Atmospheric Remote Sensing, Wuhan 430072, China  
Full list of author information is available at the end of the article

### Graphical Abstract



### Introduction

Atmospheric circulation shows distinguishable features among low, middle and high latitudinal zones owing to the differences in solar radiation, and the atmosphere is characterized by the layered structure in thermal and ionizing properties because of the differences in solar radiation absorption (Andrews et al. 1987; Saha 2008). There are numerous dynamical and thermodynamic processes with different temporal and spatial scales in the atmosphere, which can excite various scale atmospheric perturbations, such as mid- and small-scale gravity waves (GWs), global-scale planetary waves (PWs) and atmospheric oscillations (Salby 1984; Fritts and Alexander 2003; Zhang 2005). As these perturbations move away from their source region, energy and momentum carried by them are transported horizontally and vertically in the atmosphere, leading to energy and momentum coupling among the different atmospheric zones and among the different atmospheric layers. Hence, atmospheric waves and oscillations play an essential role in energy and momentum budgets of the atmosphere.

In the polar atmosphere, there are maximum heating in summer polar day and maximum cooling in winter polar night, which cause dominant westward and eastward winds in the middle atmosphere over the summer and winter hemispheres due to the change in temperature gradient (Andrews et al. 1987), respectively. The polar atmospheric temperature is far from radiative equilibrium, especially in the winter lower stratosphere and upper mesosphere (Wehrbein and Leovy 1982), indicating that there exists intense dynamical heating over there. Stratospheric sudden warming (SSW) is a typical dynamical heating event in the polar atmosphere (Baldwin et al. 2021). During SSWs, the polar stratospheric mean temperature can rapidly increase by tens of degree within a

few days, and the mean zonal wind at 10 hPa poleward of 60°N decelerates and even reverses (Pawson and Naujokat 1999), which are referred to as minor or major SSW (Labitzke 1977). As the polar stratosphere is warming, cooling occurs in the mesosphere and lower thermosphere (MLT) at high-latitudes and in the stratosphere at mid- and low-latitudes (Liu and Roble 2005; Yuan et al. 2012; Sox et al. 2016), thus SSWs have an influence at least on the middle atmosphere over the hemisphere. It is generally accepted that amplification of upward propagating PWs and their interaction with the mean flow play a key role in the initiation and progression of SSWs (Matsuno 1971; Liu and Roble 2002). During SSWs, quasi-16-day wave (Q16DW) activity is a relatively common phenomenon (Dowdy et al. 2007; Pancheva et al. 2008; Vineeth et al. 2009; Chandran et al. 2013; Gong et al. 2019; Yu et al. 2019).

In classical PW theory, Q16DW is identified as the zonal wavenumber  $s=1$ , westward propagating second symmetric Rossby mode, and its period and three-dimensional structure may be modified by the variation of the background wind and temperature fields (Salby 1981a, 1984). In theoretical prediction and experimental observations, Q16DWs generally have a period range of about 12–20 days (Salby 1981b; Luo et al. 2002a; Day and Mitchell 2010; Huang et al. 2013). Q16DW in the MLT has been investigated from ground-based radar and satellite-borne instrument observations (Forbes and Leveroni 1992; Forbes et al. 1995; Williams and Avery 1992; Espy and Witt 1996; Espy et al. 1997; Mitchell et al. 1999; Luo et al. 2000, 2002a, b; Namboothiri et al. 2002; Jiang et al. 2005; Lima et al. 2006; Day and Mitchell 2010; McDonald et al. 2011). On an average, the wave activity is more pronounced in the zonal wind than in the meridional wind. In the MLT at mid-latitudes, Q16DW was

reported to be the strongest in winter with a zonal wind amplitude of over  $10 \text{ ms}^{-1}$  and the temperature amplitude of up to 5 K, and the weakest in summer with the maximum amplitude of about  $6\text{--}7 \text{ ms}^{-1}$  ( $2\text{--}3 \text{ K}$ ) in the zonal wind (temperature) derived from bandpass filtering with periods of 12–20 days (Forbes et al. 1995; Luo et al. 2002a, b; Jiang et al. 2005; Day and Mitchell 2010). Because of small phase speed, wave propagation depends on the background wind, thus Q16DW in the summer hemisphere was proposed to be ducted from the winter hemisphere along the zero wind line, or be in situ excited in the MLT due to energy and momentum deposition of GWs modulated by Q16DW in the troposphere and lower stratosphere (Forbes et al. 1995; Miyoshi 1999; Lima et al. 2006). In the mesopause region, Q16DW usually shows very slow or no obvious phase changes with height, implying a considerably large vertical wavelength and even a standing wave structure in the MLT (Luo et al. 2002a, 2002b; Namboothiri et al. 2002; Jiang et al. 2005; Lima et al. 2006; McDonald et al. 2011).

With the development of atmospheric detection technology, more westward and eastward propagating Q16DW modes were observed (Shepherd and Tsuda 2008; Kleinknecht et al. 2014). Westward propagating waves, particularly zonal wavenumber  $s=1$  mode, are stronger than eastward propagating waves in the stratosphere and mesosphere in the Northern Hemisphere (Meek and Manson 2009; Pancheva et al. 2009). However, it was also reported that in the Northern Hemisphere, westward and eastward propagating wavenumber  $s=1$  Q16DWs are the dominant modes with similar magnitudes, while in the Southern Hemisphere, eastward propagating wavenumber  $s=1$  and 2 waves are more intense than westward propagating wave modes (Alexander and Shepherd 2010; McDonald et al. 2011). The different results were attributed to the large interannual variability of the Q16DW activity (McDonald et al. 2011). Numerous studies have revealed that westward propagating wavenumber  $s=1$  Q16DW is generally associated with vortex displacement-type SSWs, whereas westward propagating wavenumber  $s=2$  mode is related to vortex split-type SSWs despite that wavenumber  $s=1$  mode is also involved in SSWs in most split-type events (Charlton and Polvani 2007; Gong et al. 2019).

It is interesting that the winter of 2013/2014 was characterized by the continuous predominance of wavenumber  $s=2$  PW in the stratosphere with the vertical component of Eliassen–Palm (EP) flux almost equal to the highest value in the winter of 2008/2009 derived from the 55-year reanalysis data (Harada and Hirooka 2017), but only a minor SSW took place in early February 2014 relative to a strong split-type major SSWs in January 2009 driven by wavenumber  $s=2$  PW (Manney et al.

2009; Wang et al. 2016; Harada and Hirooka 2017). The development and continuance of the quasi-barotropic Aleutian high pressure were proposed to be an important reason for the lack of major SSW in this winter (Wang et al. 2014; Harada and Hirooka 2017). The anomalous high pressure emerged from persistent energy of Rossby wave in the North Pacific due to the significant anomalies of sea surface temperature pattern from the middle of 2013, thus the pressure anomalies began in the autumn and then were subsequently intensified into the winter, causing severe cold in North America and drought over California in the winter (Wang et al. 2014; Yu and Zhang 2015; Hartmann 2015; van Oldenborgh et al. 2015). This is also consistent with the result that the responses of atmospheric humidity, precipitation and temperature lag behind sea surface temperature changes in the Pacific by about 2–3 months (Li et al. 2018; Du et al. 2021). Hence, there are abnormal precipitation and temperature in the lower atmosphere, and extraordinary wavenumber  $s=2$  PW activity and SSW event in the stratosphere in the winter of 2013/2014. In this paper, we present an extraordinary Q16DW activity from the troposphere to the MLT over the Northern Hemisphere with an onset in the autumn of 2013, which lasts until January 2014, but is distinguished from the Q16DW activity during the SSW starting in early February 2014.

In next section, meteor radar observations are briefly described. In “Results” section, the extraordinary Q16DW activity and the other one in the SSW events are studied from the radar observations and reanalysis data. The dynamical processes associated with the two Q16DW activities are discussed in “Discussion” section, and “Conclusion” section provides the conclusion of this study.

## Data

The horizontal winds from two meteor radars arranged approximately along the  $115^\circ\text{E}$  meridian line for 7 years from October 2010 to September 2017 are utilized to investigate the correlation between the strong PW activities in the MLT and the SSW events, and the radar observations between 1 September 2013 and 1 April 2014 are used to analyze two Q16DW activities in detail.

The two meteor radars are located at Beijing (BJ,  $40.3^\circ\text{N}$ ,  $116.2^\circ\text{E}$ ) and Wuhan (WH,  $30.5^\circ\text{N}$ ,  $114.6^\circ\text{E}$ ), in China, established by the Institute of Geology and Geophysics, Chinese Academy of Sciences (IGGCAS) through the support of the Chinese Meridian Project. The radars are an all-sky interferometric meteor radar (SKiYMET) system (Hocking et al. 2001) with a same operating frequency of 38.5 MHz. The trails of meteor ablation are illuminated by a three-element Yagi antenna directed toward the zenith with a transmitted peak power

of 7.5 kW, and the echoes reflected by meteor trails are detected by five three-element Yagi antennas oriented along two orthogonal baselines. The detailed technical specifications of the radar system were presented in early works (Xiong et al. 2013; Yu et al. 2015; Huang et al. 2019). These meteor radars can provide horizontal wind in the height range of 70–110 km with a temporal resolution of 1 h and a vertical resolution of 2 km. The measurement uncertainty is typically  $2\text{--}4\text{ ms}^{-1}$  in the horizontal wind data, and the estimation of wind velocity and uncertainty observed by the SKiYMET radar can be found in previous studies (Hocking et al. 2001; Franke et al. 2005). The number of meteor counts detected by the radars showed a strong dependence on height, with an approximate Gaussian distribution centered at about 88 km, thus the wind data availability is high around this height. The zonal and meridional winds in the height range of 76–100 km were utilized in our study. In the 7 years, there are two long observational gaps at WH, whereas, in the time period from 1 September 2013 to 1 April 2014 that we focus on, the missing data are little with a fraction smaller than 2% at 88 km. The missing data are interpolated linearly, thus the radar observations are suitable for investigating the PW with a long period of about 16 days.

We examine the evolution of stratospheric temperature and wind based on the reanalysis data from the Modern-Era Retrospective Analysis for Research and Applications version 2 (MERRA2), which is produced by the Goddard Earth Sciences Data and Information Services Center (GES DISC) of the National Aeronautics and Space Administration (NASA). Relative to the previous version, the improvements of MERRA2 are presented in detail by Molod et al. (2015), and subsequently, an overview of MERRA2 is reported by Gelaro et al. (2017). The MERRA2 reanalysis data can be freely accessible from the website at <https://gmao.gsfc.nasa.gov/reanalysis/MERRA-2/>. The reanalysis data are 6-hourly instantaneous analysis fields on a  $0.5^\circ \times 0.625^\circ$  latitude-by-longitude grid at 72 pressure levels from the ground up to 0.01 hPa level.

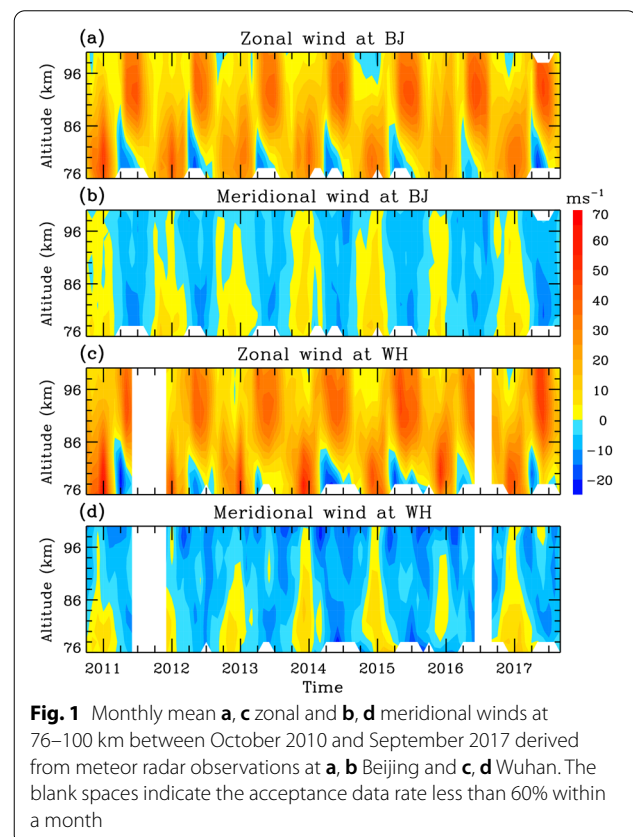
The upper bound of 0.01 hPa in the reanalysis data corresponds to the altitudes of about 78–80 km. By comparing the extracted Q16DWs at 0.01 hPa in the reanalysis data and at 78–80 km in the radar data, we will see that in the zonal winds, the wave phases are in good agreement with each other in the two datasets, and the wave amplitudes are slightly smaller from the reanalysis data than from the radar observations. Relative to in the zonal winds, both the wave amplitudes and phases in the meridional winds show a less consistency between the two datasets. Hence, we should keep in mind that the results from the reanalysis data cannot take the place

of those from the observations, and the results deserve more attention in the reanalysis zonal wind than in the reanalysis meridional wind.

## Results

### Q16DW in meteor observation

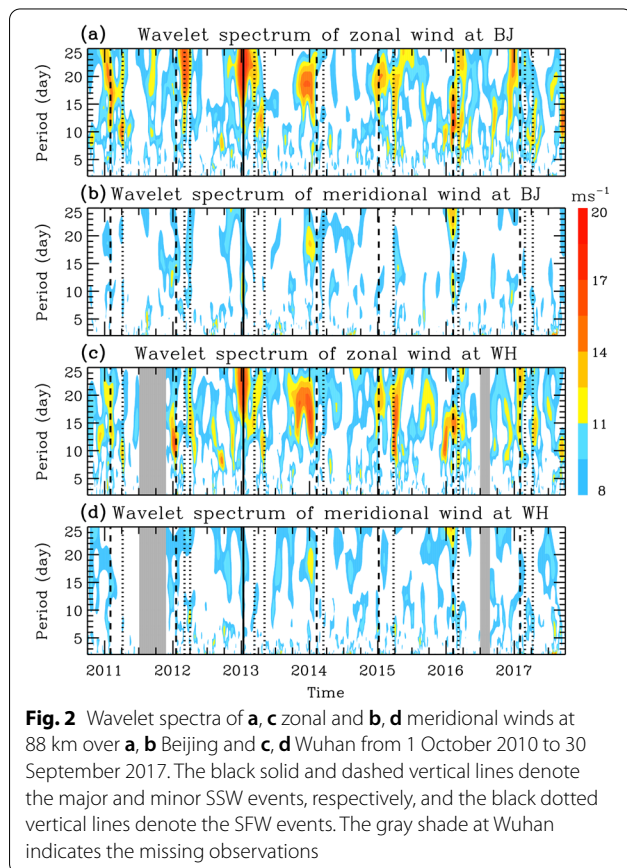
Figure 1 shows the monthly mean zonal (positive eastward) and meridional (positive northward) winds at the height range of 76–100 km observed by the meteor radars at BJ and WH for 7 years from October 2010 to September 2017. At WH, the observational data are missing in two long periods of 4 July–23 November 2011 (143 days), and 1 July–22 August 2016 (53 days). The zonal wind in the MLT at mid-latitudes exhibits an interesting feature of two annual oscillations. One oscillation is centered at about 92 km with the maximum velocity of about  $40\text{--}50\text{ ms}^{-1}$  at the two stations in the transition from spring (March–May) to summer (June–August), and the other is centered around 80 km with the maximum value of about  $40\text{--}50\text{ ms}^{-1}$  ( $50\text{--}65\text{ ms}^{-1}$ ) at BJ (WH) in winter (December–March). Because the two annual oscillations are nearly out of phase, the zonal wind at the height of 80–92 km shows a distinguishable semi-annual oscillation. Relative to the zonal wind, the meridional wind is weak with the monthly mean values of about





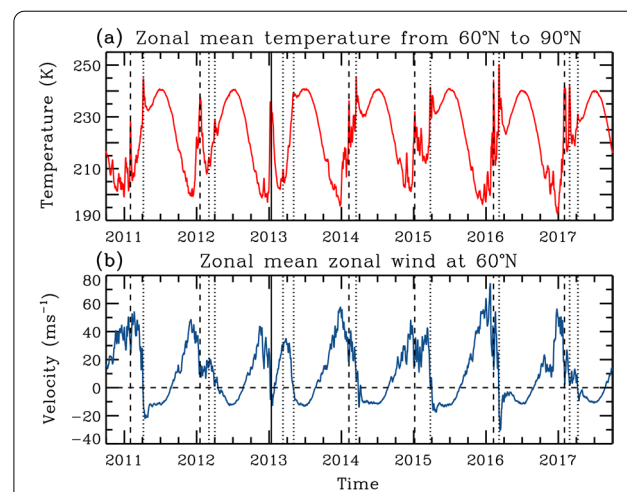
– 15 to 10  $\text{ms}^{-1}$ , and the northward wind arises mainly in autumn (September–November) and early winter.

The missing data are minimal at 88 km with a fraction less than 2% (except the two data gaps at WH) due to the Gaussian meteor number distribution centered at this height, thus the winds at 88 km have good representation and high reliability. For investigating the PW activities, we use linear interpolation to fill in the missing data, and then perform a wavelet transform on the zonal and meridional winds at 88 km to obtain the dominant PW modes and the temporal variability of these modes. Morlet wavelet function consisting of a plane wave modulated by a Gaussian envelope is chosen as mother wavelet (Huang et al. 2015; Cheng et al. 2021), and we follow Torrence and Compo (1998) to carry out the wavelet transform with the width of Morlet wavelet function defined as the  $e$ -folding time of wavelet amplitude. Figure 2 presents the wavelet spectra of the zonal and meridional winds at 88 km during the 7 years. One can note that the perturbations with temporal scales of PWs and short-period oscillations are robust in the MLT during winter, similar to the observations from the Super Dual Auroral Radar Network (SuperDARN) radars at latitudes of 51°–66°N (Kleinknecht et al., 2014). As is



well known, PW activities are usually associated with SSWs, thus we calculate the daily averaged zonal mean temperature at 10 hPa between 60°N and 90°N and the daily averaged zonal mean zonal wind at 10 hPa over 60°N from 1 October 2010 to 30 September 2017 based on the MERRA2 reanalysis data, which are depicted in Fig. 3. The SSW events are easy to identify from the mean temperature between 60°N and 90°N, and then the major and minor SSWs are distinguished by whether the zonal wind at 60°N reverses or not. We mark the date of the maximum temperature in the major and minor SSWs with the black solid and dashed vertical lines in Figs. 2 and 3, respectively. Stratospheric final warming (SFW) is indicative of the final transition of stratospheric winter circulation from eastward to westward (Andrews et al. 1987). In terms of zonal wind anomalies, SFW is to a certain extent similar to the major SSW; whereas, SFW is still substantially different from the major SSW because the polar winter vortex collapses and the reversed mean zonal wind does not return back until the next transition from summer to autumn (Black and McDaniel 2007). SFW may be a strong warming, and may also consist of several successive weak warming events (Yu et al. 2019). The SFW is marked by the dotted vertical line in Figs. 2 and 3.

It can clearly be seen from Fig. 2 that the PW and oscillation activities in the MLT at mid-latitudes have a close relationship with the SSWs and SFWs. In the 7 years, only a major SSW takes place around 11 January 2013, and correspondingly, an oscillation with a wide period range centered at 22 days is the strongest



perturbation in the zonal winds, with the spectral amplitudes of  $19.2 \text{ ms}^{-1}$  ( $17.3 \text{ ms}^{-1}$ ) at BJ (WH). Generally, the perturbations are considerably weak in the meridional wind relative to in the zonal wind. However, it is interesting that there are PW activities from the autumn of 2013 to the winter of 2013/2014, which seem not to have much relevance to the SSW and SFW in the winter. The PW is strong not only in the zonal wind, but also in the meridional wind, and lasts for a longer duration compared with the other PWs during the SSW and SFW events. In addition, there are no prominent PW activities around the SSW on 9 February 2014 and the SFW on 16 March 2014, which is different from the scenario in the SSW and SFW in the other years.

In order to clearly show the PW evolution with time, the wavelet spectra of the zonal and meridional winds at 88 km from 1 September 2013 to 1 April 2014 are replotted in Fig. 4. In the zonal wind, the PW is active for a long time of nearly 4 months from about October 2013 to January 2014, and has a period range of about 14–20 days, thus we call it Q16DW. The Q16DW intensity decays rapidly from about 21 January 2014, which is obviously earlier than the temperature peak of the SSW on 9 February 2014, and even the onset of the SSW on 4 February 2014. In the meridional wind, the strong Q16DW occurs mainly in December 2013 and January 2014. Overall, the Q16DW onset in both the zonal and meridional winds at WH predates that at BJ. The spectral amplitude has the maximum values of  $15.9 \text{ ms}^{-1}$  in the zonal wind and  $12.7 \text{ ms}^{-1}$  in the meridional wind at

BJ, and the similar magnitudes of  $17.3 \text{ ms}^{-1}$  in the zonal wind and  $12.2 \text{ ms}^{-1}$  in the meridional wind at WH.

Since the Q16DW strength in the zonal wind is slightly stronger at WH than at BJ, we use the MERRA2 reanalysis data at WH to highlight the Q16DW activity from the troposphere to the stratosphere. The wavelet transform is carried out on the reanalysis zonal wind at WH between 1 September 2013 and 1 April 2014. Figure 5 presents the wavelet spectra at the selected pressure levels. The pressure levels at 375, 56, 10, 2.6, 1.6 and 0.6 hPa correspond approximately to the altitudes at about 7, 20, 32, 40, 45 and 52 km derived from logarithmic pressure height formula under a specified scale height of 7 km, respectively. Figure 5 illustrates that the Q16DW arises in the zonal wind from the troposphere to the stratosphere, and is intense in November and December 2013. Besides, the Q16DW activities can also be seen around the SSW and SFW events. Nevertheless, the later event seems to be another Q16DW event distinguished from the earlier one because their spectrum peaks not only are separated from each other in time, but also show the different evolutions with height. It can be noted from Fig. 4 that in the zonal wind of the MLT, the corresponding Q16DW occurs during the earlier interval, but seems not to obviously arise during the later interval.

#### Q16DW propagation

With the help of the reanalysis data, we investigate the propagation features of these Q16DWs. By using a band-pass filter with lower and upper cut-off periods of 12.5 and 20 days, the Q16DWs are extracted from the radar

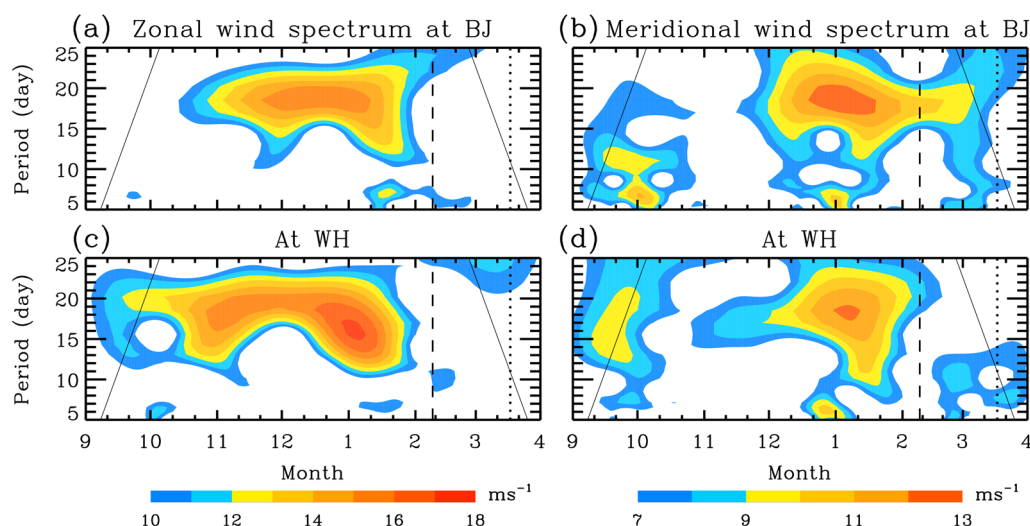


**Fig. 4** Wavelet spectra of **a, c** zonal and **b, d** meridional winds at 88 km between 1 September 2013 and 1 April 2014 from meteor radar observations over **a, b** Beijing and **c, d** Wuhan. The black dashed and dotted vertical lines denote the minor SSW and SFW events, respectively. The tilted solid lines denote the cone of influence for the wavelet analysis

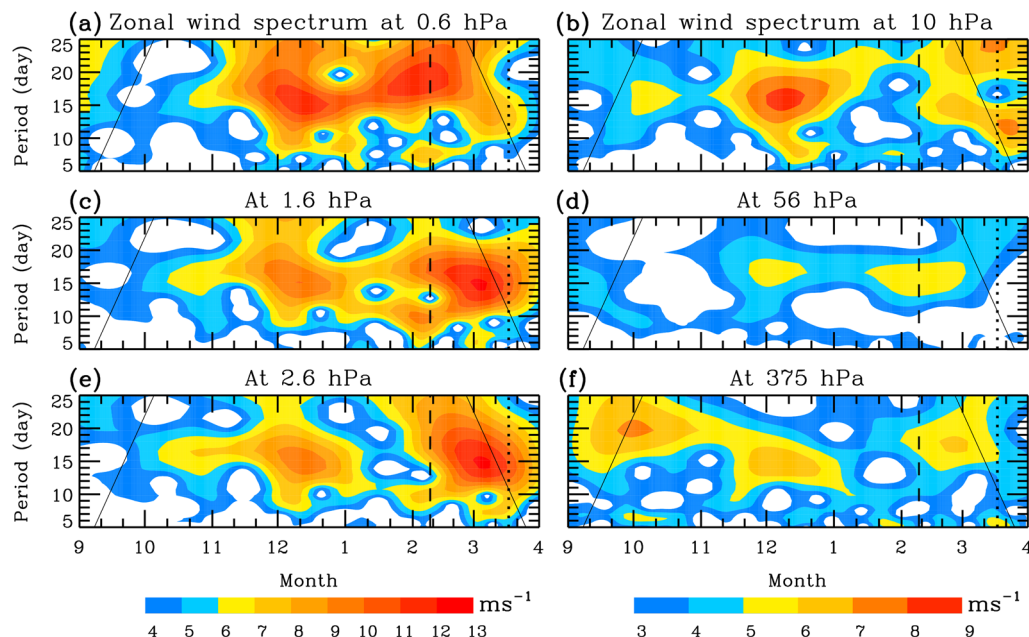


**Fig. 5** Wavelet spectra of zonal wind at **a** 0.6, **c** 1.6, **e** 2.6, **b** 10, **d** 56 and **f** 375 hPa levels over Wuhan based on MERRA2 reanalysis data from 1 September 2013 to 1 April 2014. The pressure levels of 375, 56, 10, 2.6, 1.6 and 0.6 hPa correspond to the altitudes of about 7, 20, 32, 40, 45 and 52 km, respectively. The black dashed and dotted vertical lines denote the minor SSW and SFW events, respectively. The tilted solid lines denote the cone of influence for the wavelet analysis

observations at 78–98 km and the MERRA2 reanalysis data at  $10^3$ – $10^{-2}$  hPa levels ( $\sim 0$ –80 km) between 1 September 2013 and 1 April 2014. Figure 6 shows the filtered Q16DW in the zonal and meridional winds at BJ and WH. The upper bound at  $10^{-2}$  hPa level in the reanalysis data is approximately around the altitude of 80 km, thus we can see that the Q16DWs at 78 and 80 km in the radar observations are largely in agreement with those at  $10^{-2}$  hPa in the reanalysis data, in particular, the consistency of their phases, which shows the reliability of the two datasets. Due possibly to the limitation of observational data used in assimilation to produce the reanalysis data, the Q16DW magnitudes at  $10^{-2}$  hPa in the reanalysis are sometimes different from those at 78 and 80 km in the observation. For example, in the zonal wind at 78 and 80 km, the Q16DW activities from the radar observations obviously arise at both WH and BJ from 20 October to 10 November 2013, but the corresponding wave activities cannot clearly be seen at  $10^{-2}$  hPa from the reanalysis data. In contrast, the Q16DW occurs in the reanalysis meridional wind at  $10^{-2}$  hPa over Wuhan around the SSW event, however, the corresponding wave does not evidently appear in the observed meridional wind at 78 and 80 km. Even so, the small difference should not severely affect the wave analysis from the troposphere to the MLT. In the troposphere, the Q16DW amplitude is weak because of the dense atmosphere. In

the stratosphere and MLT, the strong Q16DW activities before the SSW are distinguishable from those around the SSW and SFW events. Before the SSW, the Q16DW displays a downward phase progression from the MLT to the stratosphere, indicating the upward propagation of the Q16DW, while after the SSW, the Q16DW phase is steeper and even progresses upward. For the extraordinary Q16DW of our concern during October 2013–January 2014, the vertical wavelength is estimated to be about 80 km in the MLT over BJ and WH based on the vertical variation of wave phase in the zonal wind at 78–98 km from the radar observations, and to be about 120 km at  $10$ – $0.1$  hPa levels ( $\sim 32$ – $64$  km) in the stratosphere and lower mesosphere from the reanalysis data, respectively.

We use the same filter to extract the Q16DWs along the longitude line of  $115^\circ\text{E}$  in the Northern Hemisphere from the reanalysis data. Figure 7 depicts the filtered Q16DWs in the zonal and meridional winds at 0.6, 10, 100 and 375 hPa levels ( $\sim 52$ , 32, 16 and 7 km) from 1 September 2013 to 1 April 2014. The two Q16DW activities show the different features of phase propagation in the meridional direction. In the stratosphere, the Q16DW around the SSW and SFW exhibits a northward phase propagation, especially in the middle and upper stratosphere at mid- and high-latitudes with a thriving activity prior to the SSW. However, the first Q16DW during October to December 2013 shows

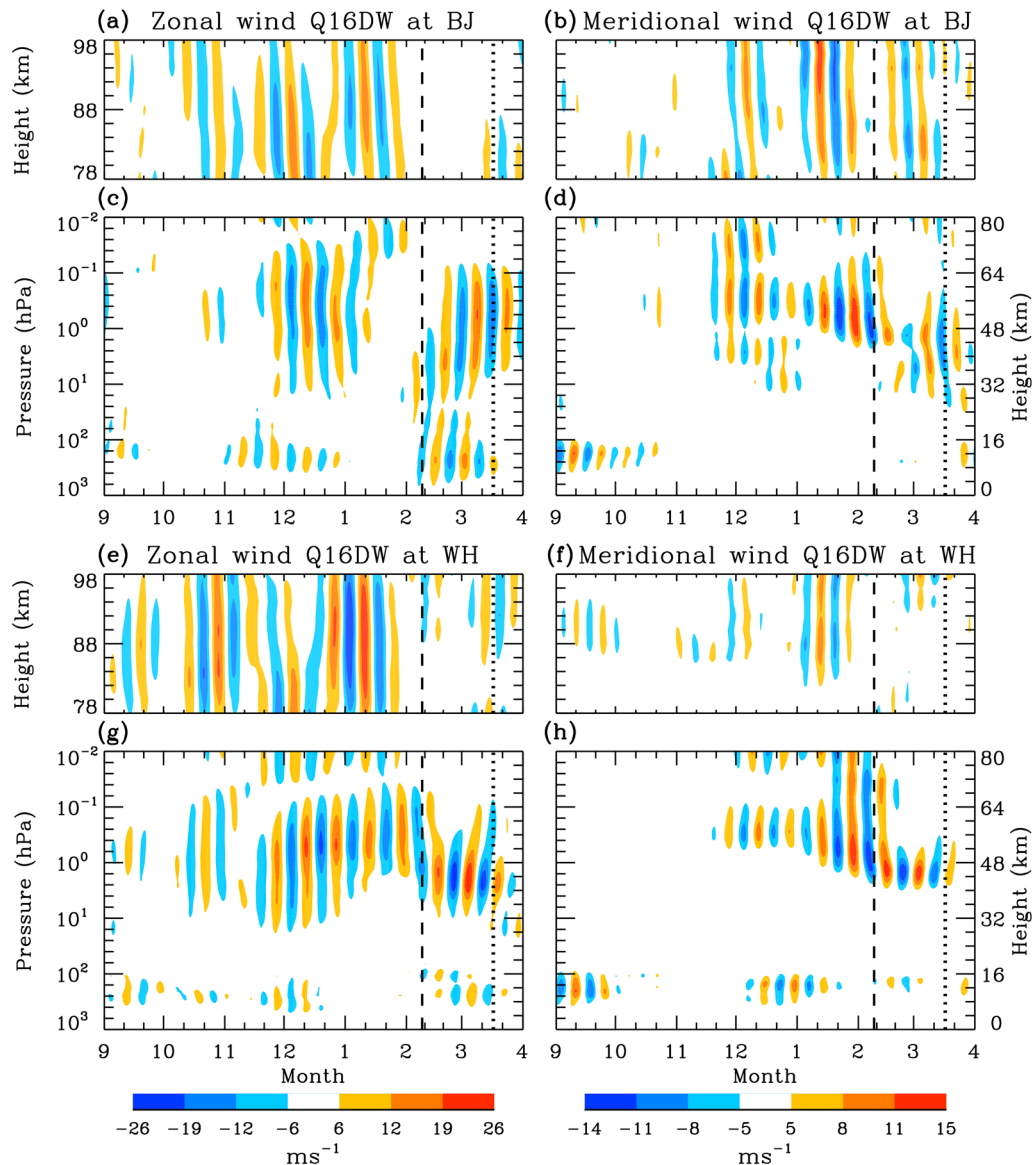


**Fig. 6** Filtered Q16DWs in (left column) zonal and (right column) meridional winds from **a, b, e, f** meteor radar observations at 78–98 km and **c, d, g, h** MERRA2 reanalysis data at  $10^{-3}$ – $10^{-2}$  hPa levels over Beijing and Wuhan during 1 September 2013–1 April 2014. For the reanalysis data, the corresponding height is marked on the right vertical axis. The band-pass filter has the lower and upper cut-off periods of 12.5 and 20 days. The black dashed and dotted vertical lines denote the minor SSW and SFW events, respectively

a southward phase progression in the troposphere, and a slow phase variation with latitude in the stratosphere at mid-latitudes. Less latitudinal change of wave phase can also be seen in the MLT at the two mid-latitudinal BJ and WH stations from Fig. 6a and e. At high-latitudes, the wave phase displays a trend of southward propagation. The characteristic of phase variation may be connected with the background condition since PW propagation is closely related to the background atmosphere.

The frequency–wavenumber spectrum can be derived from a two-dimensional Fourier transform on the reanalysis data. Based on the wavelet spectrum of the zonal wind at 0.6 hPa level ( $\sim 52$  km) in Fig. 5a, we select the zonal wind at this pressure level in the two time durations of 22 November–23 December 2013, and 20 January–20 February 2014 to perform the Fourier spectrum analysis, respectively, and then the spectral frequency is changed into the corresponding period. Figure 8 presents the period–wavenumber



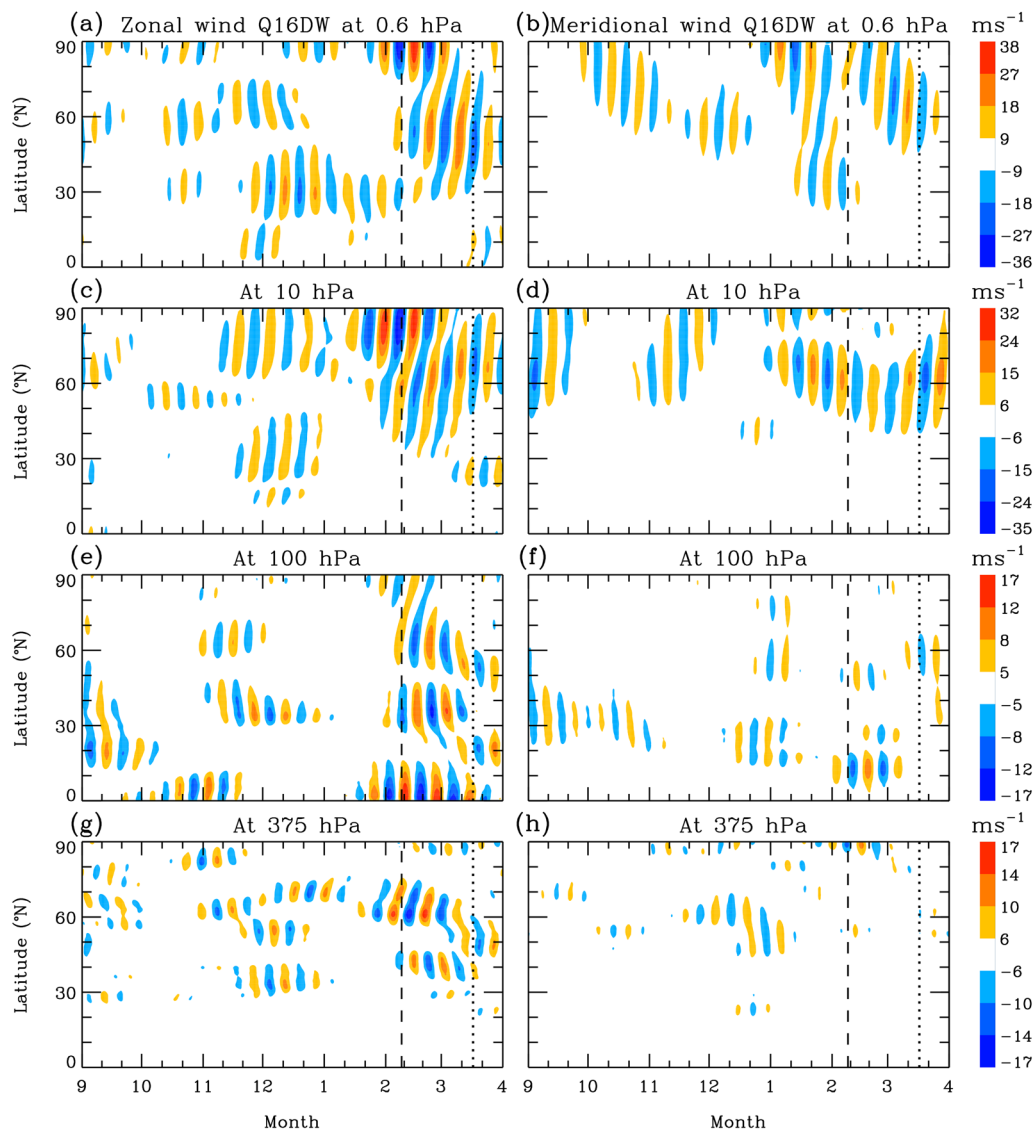


**Fig. 7** Filtered Q16DWs in (left column) zonal and (right column) meridional winds at **a, b** 0.6, **c, d** 10, **e, f** 100, and **g, h** 375 hPa levels along longitude of 115°E in Northern Hemisphere from MERRA2 reanalysis data during 1 September 2013–1 April 2014. The pressure levels of 375, 100, 10 and 0.6 hPa correspond to the altitudes of about 7, 16, 32 and 52 km, respectively. The band-pass filter has the lower and upper cut-off periods of 12.5 and 20 days. The black dashed and dotted vertical lines denote the minor SSW and SFW events, respectively

spectrum of the zonal wind perturbations obtained by removing the mean value from the reanalysis zonal wind in the two time intervals. The negative zonal wavenumber in Fig. 8 indicates the westward propagation of the wave. Interestingly, the first Q16DW has the predominant wavenumber of  $-1$  with the maximum spectral amplitude of  $8.2 \text{ ms}^{-1}$ , whereas the second Q16DW around the SSW has the predominant wavenumber of  $-2$  with the spectral magnitude of  $7.7 \text{ ms}^{-1}$ , which is consistent with the continuous predominance of PWs with wavenumber 2 in the stratosphere during

the minor SSW occurring in the winter of 2013/14 (Harada and Hirooka, 2017). Besides, in the first time duration, a spectral peak at wavenumber of  $-1$  and period of 8 days has the magnitude of  $6.2 \text{ ms}^{-1}$ . There are also other different wavenumber Q16DW components with rather weak intensity, thus the Q16DW components with wavenumbers of  $-1$  and  $-2$  are the predominant perturbations in the first and second time intervals, respectively. This indicates that the two westward propagating Q16DWs have the different zonal scales and phase speeds. Therefore, the two

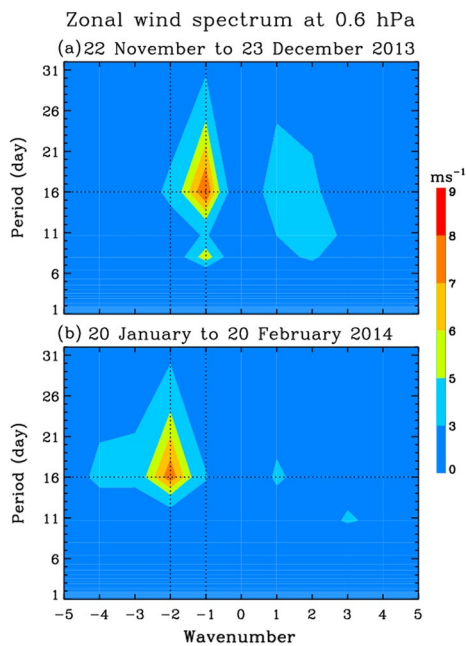


**Fig. 8** Period–wavenumber spectrum of zonal wind at 0.6 hPa level from MERRA2 reanalysis data in two time intervals of **a** 22 November–23 December 2013 and **b** 20 January–20 February 2014. The negative wavenumber represents the westward propagation of wave. The dotted horizontal line denotes the period of 16 days, and the two dotted vertical lines denote the wavenumbers of  $-1$  and  $-2$ , respectively

Q16DWs can be distinguished from not only the durations of their activities, but also the features of their propagations.

## Discussion

The vertical propagation of PWs is closely related to the background wind. The eastward zonal background wind can ensure the vertical wavenumber of PWs as a real number without imaginary part, and then is suitable for the upward propagation of PWs (Andrews et al. 1987). When the effect of the meridional variation of the mean zonal flow on the wave propagation is considered further, a refractive index is usually used to explain the propagation feature of PWs. In the region with the squared refractive index  $n^2 < 0$  PWs show the evanescent characteristic and cannot propagate freely, thus PWs can propagate in the region with  $n^2 > 0$ . The squared refractive index can be calculated from the expression of Andrews et al. (1987). In the calculation, the background wind, temperature and density are obtained by applying a running mean window with a width of 32 days moving forward in a step length of a day from the MERRA2 data; and the zonal wavenumber is chosen to be  $-1$  and  $-2$  for the first and second Q16DWs, respectively.

We calculate the zonal background winds from the radar and reanalysis data at BJ and WH by using the sliding average window. Figure 9 presents the sliding average zonal winds at BJ and WH between 1 September 2013 and 1 April 2014 from the radar and reanalysis data. Figure 10 presents the squared refractive indices at BJ and WH only for the westward propagating wavenumber 1 Q16DW, owing to the similarity of the squared indices between the westward propagating wavenumber 2 and wavenumber 1 modes. The radar observations indicate that the eastward wind dominates the zonal wind field in the height range of 78–98 km, which is appropriate for the Q16DW propagation. In the reanalysis data, the westward wind in the stratosphere arises in September 2013 and at about 20–40 km from January to March 2013, especially over WH, thus the stratospheric Q16DW in Fig. 6 is weak at these altitudes during these times. In Fig. 10, there is a thin layer at about  $4 \times 10^2 - 8 \times 10^2$  hPa with positive  $n^2$ , thus the wave enhancement in the layer can be seen from Fig. 6. In January 2014, the negative  $n^2$  in the stratosphere covers a larger height range and lasts for a longer time at BJ than at WH, causing a weaker wave at BJ relative to that at WH. Hence, although the intense Q16DW activities take place in the stratosphere from October 2013 to March 2014, the Q16DWs are decayed and even forbidden to freely travel at some heights during some specific times due to the occurrence of the westward background wind and the negative  $n^2$ .

Finally, we estimate the effects of the Q16DWs on the polar background flow by calculating Eliassen–Palm (EP) flux divergence. The EP flux and its divergence can be derived from the reanalysis data by following the expressions of Andrews et al. (1987). The zonal wind, meridional wind and potential temperature perturbations of the Q16DWs are extracted by a two-dimensional filtering with the bandpass periods of 12.5–20 days and the bandpass wavenumbers of  $-1$  and  $-2$  from the MERRA2 reanalysis data, respectively. Figure 11 presents the EP flux vector and its divergence of the Q16DWs at the chosen 4 days. In order to highlight the EP flux vector in the stratosphere, the EP flux vector in Fig. 11 is weighted by the square root of  $P_0/P$  where  $P_0 = 1000$  hPa is the pressure at the ground and  $P$  is the pressure from the reanalysis data (Salby and Callaghan 2001), and then the vertical component is multiplied by a factor of 200. Since the direction of EP flux can be regarded as the direction of wave group velocity in the longitudinal and altitudinal section (Andrews et al. 1987), Fig. 11 illustrates that the Q16DWs originate mainly from the lower atmosphere at mid- and high-latitudes, and are generally intensified in the stratosphere again due to the damping in the tropopause region. In the stratosphere, the EP flux of the

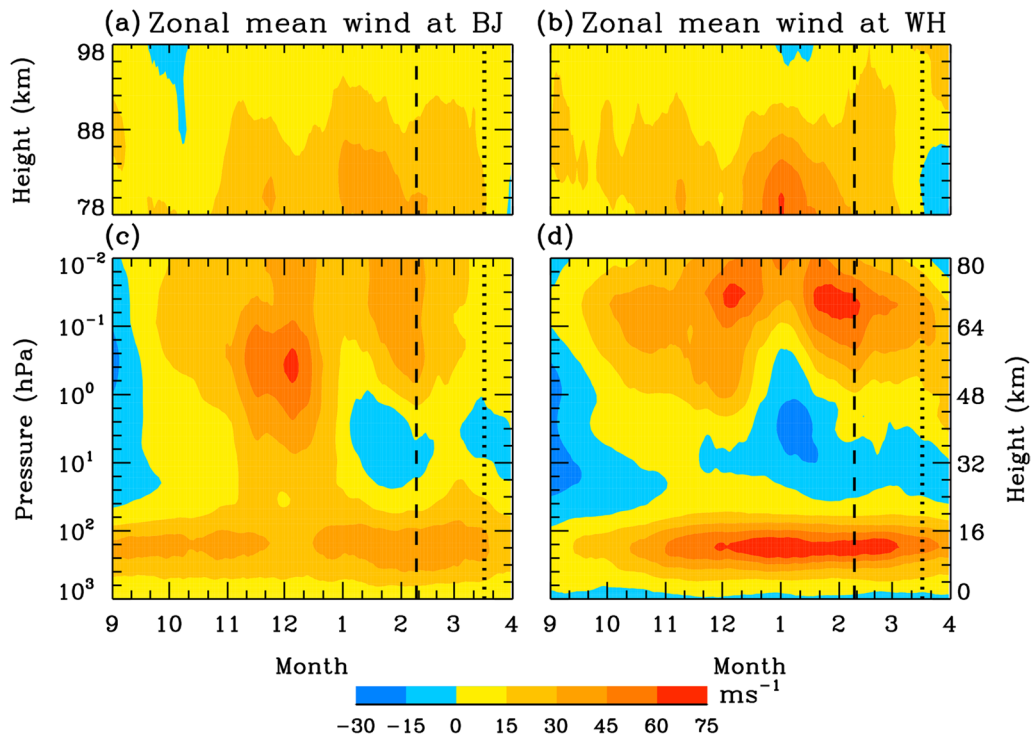


**Fig. 9** Moving average zonal winds over **a, c** Beijing and **b, d** Wuhan from 1 September 2013 to 1 April 2014 derived from **a, b** meteor radar observations at 78–98 km and **c, d** MERRA2 reanalysis data at  $10^3$ – $10^{-2}$  hPa levels. For the reanalysis data, the corresponding height is marked on the right vertical axis. The sliding window has a width of 32 days with an increment of a day. The black dashed and dotted vertical lines denote the minor SSW and SFW events, respectively

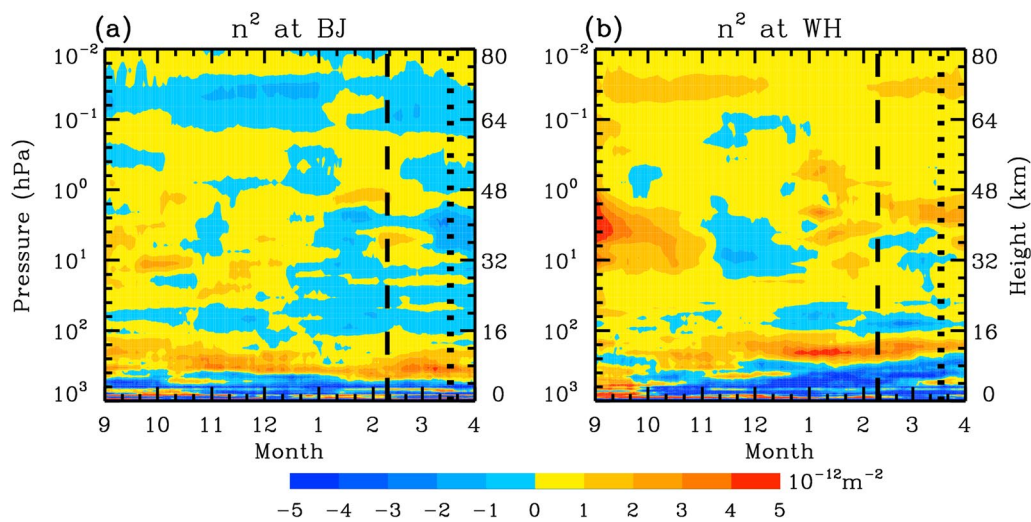


**Fig. 10** Squared refractive indices for westward propagating wavenumber 1 Q16DW over **a** Beijing and **b** Wuhan from 1 September 2013 to 1 April 2014 derived from MERRA2 reanalysis data. The corresponding height is marked on the right vertical axis. The black dashed and dotted vertical lines denote the minor SSW and SFW events, respectively

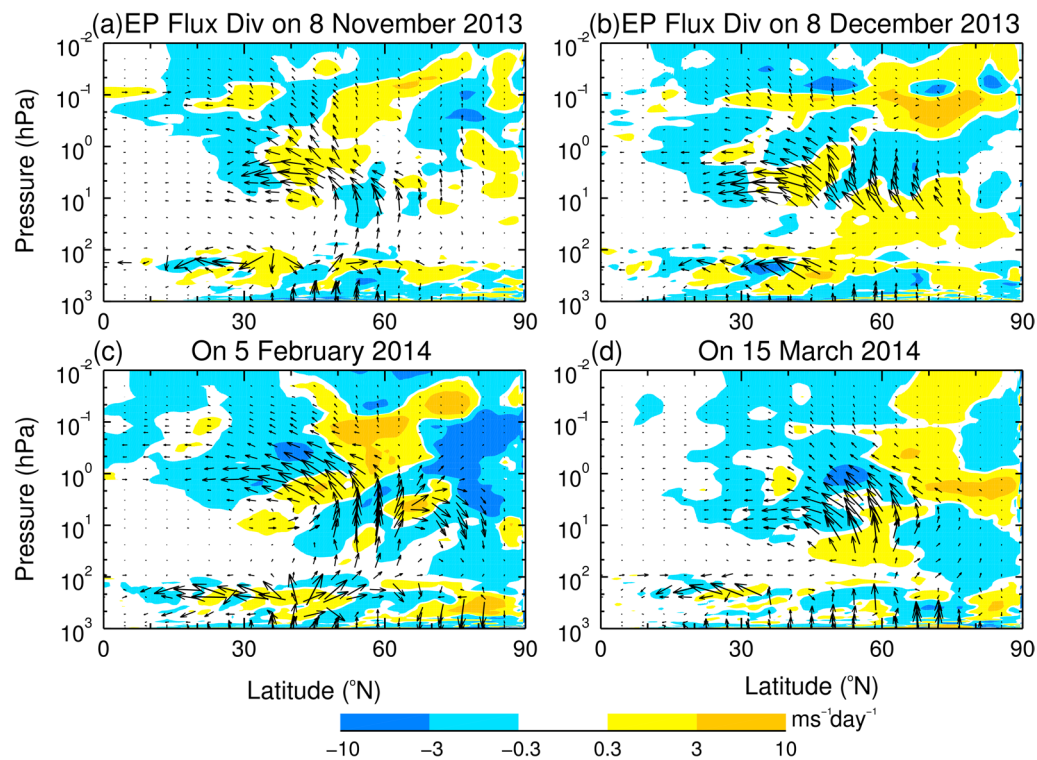


**Fig. 11** (arrow) EP flux vector and (color shading) EP flux divergence on **a** 8 November 2013, **b** 8 December 2013, **c** 5 February 2014 and **d** 15 March 2014. The EP flux vector is weighted by the square root of pressure ratio, and then the vertical component is multiplied by a factor of 200

extraordinary Q16DW in November and December 2013 shows a dominant southward transport. On the whole, the EP flux divergence is small in the polar stratosphere and tends to make a little contribution to the polar vortex intensification though there is also the negative divergence at some heights. On 5 February 2014 during the SSW, the northward EP flux has a negative divergence almost in the whole polar stratosphere, indicating that the wave plays a significant role in the SSW occurrence. On 15 March 2014 during the SFW, the northward branch of the EP flux is weak, and its divergence shows that the wave activity decreases the eastward zonal wind of the lower stratosphere. Hence, the Q16DWs in different time could have the different influences on the polar stratosphere.

## Conclusion

In this paper, we use the 7-year meteor radar observations at the two mid-latitude stations to investigate the PW and short-period oscillation activities in the MLT at mid-latitudes and the correlation between these wave and oscillation activities and the SSW events in the polar region, and find an extraordinary Q16DW which lasted for a long duration from about October 2013 to January 2014. Many previous works have statistically analyzed

the climatological feature of Q16DW. Radar measurements indicate that the Q16DW activity in the MLT lasts generally for less than 2 months with the maximum amplitude in winter, and shows a large interannual variability at mid- and high-latitudes (Mitchell et al. 1999; Luo et al. 2000, 2002a, b; Namboothiri et al. 2002). Further, the Q16DW in the MLT was suggested to occur in intermittent bursts in winter and be intermittent and weak throughout the other seasons based on the wind and temperature observations (Day and Mitchell 2010; McDonald et al. 2011), thus our spectral results support the intermittent bursts of PWs and oscillations in the MLT in winter. However, these early works did not attach the intermittent bursts of Q16DW to the SSW events, while our results indicate the intermittent bursts of PWs and oscillations in the MLT at mid-latitudes in winter are directly connected to the SSW and SFW events, except the extraordinary Q16DW activity.

On the other hand, there are numerous studies of PWs in the SSW events. These studies focused mainly on two topics: (1) amplification of PWs and then their interaction with the background flow initialize SSW, as proposed by Matsuno (1971), and influence the types and evolution of SSW (e.g., Pawson and Naujokat 1999; Liu and Roble 2002; Charlton and Polvani 2007; Manney



et al. 2009; Wang et al. 2016; Gong et al. 2019; Baldwin et al. 2021), and (2) response of PWs in the MLT to the SSW and SFW events (e.g., Dowdy et al. 2007; Pancheva et al. 2008; Vineeth et al. 2009; Yuan et al. 2012; Chandran et al. 2013; Kleinknecht et al. 2014; Yu et al. 2019). The response is clear in our spectrum results; whereas, in this study, we present a notable exception in the 7-year observations. The extraordinary Q16DW occurs in the MLT at mid-latitudes from October 2013 to January 2014 before the SSW in February 2014, meanwhile, there are not evident PW or oscillation bursts in the zonal wind of the MLT at mid-latitudes during the SSW and SFW events in February and March 2014 though a corresponding Q16DW is pronounced in the stratosphere. These results are different from the radar observations in the other years.

The wavelet transform demonstrates that the extraordinary Q16DW has the spectral amplitudes of 15.9 and 17.3  $\text{ms}^{-1}$  in the zonal wind, and the comparable magnitudes of 12.7 and 12.2  $\text{ms}^{-1}$  in the meridional wind at 88 km over BJ and WH, respectively. Nevertheless, in previous observations, the Q16DW in the MLT is usually much weaker in the meridional wind than in the zonal wind (Luo et al. 2000, 2002a, b; Namboothiri et al. 2002). The wave phase shows a downward progression from the MLT to the stratosphere, indicating that the wave propagates upward and originates from the lower atmosphere. Based on the considerably slow phase speed, the vertical wavelength is estimated to have the regional value of about 80 (120) km in the MLT (the stratosphere) over the two stations, which is largely consistent with the vertical scale and even standing wave pattern in the previous observations (Luo et al. 2000, 2002a, b; Day and Mitchell 2010; McDonald et al. 2011). Similarly, the latitudinal variation of the wave phase is also very slow. With the help of the two-dimensional Fourier transform, the Q16DW is identified to be a westward propagating wavenumber 1 mode, which is obviously distinguished from the other westward propagating wavenumber 2 Q16DW in the stratosphere during the SSW and SFW events.

From October 2013 to March 2014, the eastward winds prevail from the lower atmosphere to the MLT at the two mid-latitude sites, which is suitable for the Q16DW propagation. Even so, there are also the westward winds in the lower stratosphere in some months, especially at WH, and the intermittently negative values of the squared refractive index at some heights, in particular at BJ, thus accordingly, the Q16DWs are weakened and exhibit the evanescent feature over there. The EP flux vector of the Q16DWs indicates that these waves originate mainly from the lower atmosphere at

mid- and high-latitudes, and are obviously intensified in the middle stratosphere. The extraordinary Q16DW shows a dominant southward EP flux, and may make a little contribution to the polar vortex intensification due to the small EP flux divergence. However, for the Q16DW in the SSW event, the EP flux has a strong negative divergence almost in the whole polar stratosphere, implying an important role in the stratospheric eastward zonal wind reduction in the SSW. The northward branch of the EP flux is weak in the SFW. In this way, the Q16DWs in different durations have the different influences on the polar stratosphere.

Finally, some investigations revealed many abnormal phenomena from the autumn of 2013 to the winter of 2013/2014. There are anomalous sea surface temperature pattern, Aleutian high pressure and persistent Rossby wave from the middle of 2013 (Wang et al. 2014; Hartmann 2015), which leads to severe cold in North America and drought over California in the winter (Yu and Zhang 2015; van Oldenborgh et al. 2015). In the stratosphere, the strong wavenumber  $s=2$  PW has the very large vertical component of EP flux in the winter, but only a minor SSW rather than a split-type major SSW arises in February 2014 (Harada and Hirooka 2017). The extraordinary Q16DW is possibly associated with the anomalous sea surface temperature and persistent Rossby wave since the Q16DW is also relatively active in the troposphere during this period.

#### Acknowledgements

We are grateful to the editor and anonymous reviewers for their valuable comments on our paper. We thank the IGGCAS and the Chinese Meridian Project for providing meteor radar data, and the NASA GES DISC for providing MERRA2 reanalysis data.

#### Author contributions

KH and XH proposed the scientific ideas. XH and KH completed the analysis and the manuscript. SZ, CH YG and HC discussed the results in the manuscript. All authors read and approved the final manuscript.

#### Funding

This work was jointly supported by the National Natural Science Foundation of China under Grant Numbers 42174189, 41974176 and 42127805.

#### Availability of data and materials

The meteor radar data are accessed from the websites at <http://geospace.geodata.cn/>, and the MERRA2 reanalysis data at <https://gmao.gsfc.nasa.gov/reanalysis/MERRA-2/>.

#### Declarations

#### Competing interests

The authors declare that they have no competing interests.

#### Author details

<sup>1</sup>School of Electronic Information, Wuhan University, Wuhan, China. <sup>2</sup>Key Laboratory of Geospace Environment and Geodesy, Ministry of Education, Wuhan, China. <sup>3</sup>State Observatory for Atmospheric Remote Sensing, Wuhan 430072, China.

Received: 29 January 2022 Accepted: 8 June 2022

Published online: 23 June 2022

## References

- Alexander SP, Shepherd MG (2010) Planetary wave activity in the polar lower stratosphere. *Atmos Chem Phys* 10(2):707–718. <https://doi.org/10.5194/acp-10-707-2010>
- Andrews DG, Holton JR, Leovy CB (1987) *Middle atmosphere dynamics*. Elsevier, New York
- Baldwin MP, Ayarzagüena B, Birner T, Butchart N, Butler, AH, Charlton-Perez, AJ et al (2021) Sudden stratospheric warmings. *Rev Geophys* 59(1):e2020RG000708. <https://doi.org/10.1029/2020RG000708>
- Black RX, McDaniel BA (2007) The dynamics of Northern Hemisphere stratospheric final warming events. *J Atmos Sci* 64(8):2932–2946. <https://doi.org/10.1175/JAS3981.1>
- Chandran A, Garcia RR, Collins RL, Chang LC (2013) Secondary planetary waves in the middle and upper atmosphere following the stratospheric sudden warming event of January 2012. *Geophys Res Lett* 40(9):1861–1867. <https://doi.org/10.1002/grl.50373>
- Charlton AJ, Polvani LM (2007) A new look at stratospheric sudden warmings. Part I: climatology and modeling benchmarks. *J Clim* 20(3):449–469. <https://doi.org/10.1175/JCLI3996.1>
- Cheng H, Huang K, Liu AZ, Zhang S, Huang C, Gong Y (2021) A quasi-27-day oscillation activity from the troposphere to the mesosphere and lower thermosphere at low latitudes. *Earth Planets Space* 73:183. <https://doi.org/10.1186/s40623-021-01521-1>
- Day KA, Mitchell NJ (2010) The 16-day wave in the Arctic and Antarctic mesosphere and lower thermosphere. *Atmos Chem Phys* 10(3):1461–1472. <https://doi.org/10.5194/acp-10-1461-2010>
- Dowdy AJ, Vincent RA, Tsutsumi M, Igarashi K, Murayama Y, Singer W et al (2007) Polar mesosphere and lower thermosphere dynamics: 2. Response to sudden stratospheric warmings. *J Geophys Res Atmos* 112:D17105. <https://doi.org/10.1029/2006JD008127>
- Du M, Huang K, Zhang S, Huang C, Gong Y, Yi F (2021) Water vapor anomaly over the tropical western Pacific in El Niño winters from radiosonde and satellite observations and ERA5 reanalysis data. *Atmos Chem Phys* 21(17):13553–13569. <https://doi.org/10.5194/acp-21-13553-2021>
- Espy PJ, Witt G (1996) Observation of a quasi 16-day oscillation in the polar summer mesospheric temperature. *Geophys Res Lett* 23(10):1071–1074. <https://doi.org/10.1029/96GL01068>
- Espy PJ, Stegman J, Witt G (1997) Interannual variations of the quasi-16-day oscillation in the polar summer mesospheric temperature. *J Geophys Res Atmos* 102(D2):1983–1990. <https://doi.org/10.1029/96JD02717>
- Forbes JM, Leveroni S (1992) Quasi 16-day oscillation in the ionosphere. *Geophys Res Lett* 19(10):981–984. <https://doi.org/10.1029/92GL00399>
- Forbes JM, Hagan ME, Miyahara S, Vial F, Manson AH, Meek CE, Portnyagin YI (1995) Quasi 16-day oscillation in the mesosphere and lower thermosphere. *J Geophys Res Atmos* 100(D5):9149–9163. <https://doi.org/10.1029/94JD02157>
- Frankle SJ, Chu X, Liu AZ, Hocking WK (2005) Comparison of meteor radar and Na Doppler lidar measurements of winds in the mesopause region above Maui, Hawaii. *J Geophys Res Atmos* 110:D09S02. <https://doi.org/10.1029/2003JD004486>
- Fritts DC, Alexander MJ (2003) Gravity wave dynamics and effects in the middle atmosphere. *Rev Geophys* 41(1):1003. <https://doi.org/10.1029/2001RG000106>
- Gelaro R, McCarty W, Suárez MJ, Todling R, Molod A, Takacs L et al (2017) The modern-era retrospective analysis for research and applications, version 2 (MERRA-2). *J Clim* 30(14):5419–5454. <https://doi.org/10.1175/JCLI-D-16-0758.1>
- Gong Y, Wang H, Ma Z, Zhang S, Zhou Q, Huang C, Huang K (2019) A statistical analysis of the propagating quasi 16-day waves at high latitudes and their response to sudden stratospheric warmings from 2005 to 2018. *J Geophys Res Atmos* 124(23):12617–12630. <https://doi.org/10.1029/2019JD031482>
- Harada Y, Hirooka T (2017) Extraordinary features of the planetary wave propagation during the boreal winter 2013/2014 and the zonal wave number two predominance. *J Geophys Res Atmos* 122(21):11374–11387. <https://doi.org/10.1002/2017JD027053>
- Hartmann DL (2015) Pacific sea surface temperature and the winter of 2014. *Geophys Res Lett* 42(6):1894–1902. <https://doi.org/10.1002/2015GL063083>
- Hocking WK, Fuller B, Vandeppeer B (2001) Real-time determination of meteor-related parameters utilizing modern digital technology. *J Atmos and Sol Terr Phys* 63:155–169. [https://doi.org/10.1016/S1364-6826\(00\)00138-3](https://doi.org/10.1016/S1364-6826(00)00138-3)
- Huang KM, Liu AZ, Zhang SD, Yi F, Huang CM, Gan Q et al (2013) A nonlinear interaction event between a 16-day wave and a diurnal tide from meteor radar observations. *Ann Geophys* 31(11):2039–2048. <https://doi.org/10.5194/angeo-31-2039-2013>
- Huang KM, Liu AZ, Zhang SD, Yi F, Huang CM, Gan Q et al (2015) Observational evidence of quasi-27-day oscillation propagating from the lower atmosphere to the mesosphere over 20°N. *Ann Geophys* 33(10):1321–1330. <https://doi.org/10.5194/angeo-33-1321-2015>
- Huang KM, Xi Y, Wang R, Zhang SD, Huang CM, Gong Y, Cheng H (2019) Signature of a quasi 30-day oscillation at midlatitude based on wind observations from MST radar and meteor radar. *J Geophys Res Atmos* 124(21):11266–11280. <https://doi.org/10.1029/2019JD031170>
- Jiang GY, Xiong JG, Wan WX, Ning BQ, Liu LB, Vincent RA, Reid I (2005) The 16-day waves in the mesosphere and lower thermosphere over Wuhan (30.6°N, 114.5°E) and Adelaide (35°S, 138°E). *Adv Space Res* 35(11):2005–2010. <https://doi.org/10.1016/j.asr.2005.03.011>
- Kleinknecht NH, Espy PJ, Hibbins RE (2014) The climatology of zonal wave numbers 1 and 2 planetary wave structure in the MLT using a chain of Northern Hemisphere SuperDARN radars. *J Geophys Res Atmos* 119:1292–1307. <https://doi.org/10.1002/2013JD019850>
- Labitzke K (1977) Interannual variability of the winter stratosphere in the Northern Hemisphere. *Mon Weather Rev* 105(6):762–770. [https://doi.org/10.1175/1520-0493\(1977\)105%3c0762:VOTWS%3e2.0.CO;2](https://doi.org/10.1175/1520-0493(1977)105%3c0762:VOTWS%3e2.0.CO;2)
- Li Z, Li Y, Bonsal B, Manson AH, Scaff L (2018) Combined impacts of ENSO and MJO on the 2015 growing season drought on the Canadian Prairies. *Hydrol Earth Syst Sci* 22(10):5057–5067. <https://doi.org/10.5194/hess-22-5057-2018>
- Lima LM, Batista PP, Clemesha BR, Takahashi H (2006) 16-day wave observed in the meteor winds at low latitudes in the Southern Hemisphere. *Adv Space Res* 38(11):2615–2620. <https://doi.org/10.1016/j.asr.2006.03.033>
- Liu HL, Roble RG (2002) A study of a self-generated stratospheric sudden warming and its mesospheric-lower thermospheric impacts using the coupled TIME-GCM/CCM3. *J Geophys Res Atmos* 107(D23):4695. <https://doi.org/10.1029/2001JD001533>
- Liu HL, Roble RG (2005) Dynamical coupling of the stratosphere and mesosphere in the 2002 Southern Hemisphere major stratospheric sudden warming. *Geophys Res Lett* 32:L13804. <https://doi.org/10.1029/2005GL022939>
- Luo Y, Manson AH, Meek CE, Meyer CK, Forbes JM (2000) The quasi 16-day oscillations in the mesosphere and lower thermosphere at Saskatoon (52°N, 107°W), 1980–1996. *J Geophys Res Atmos* 105(D2):2125–2138. <https://doi.org/10.1029/1999JD900979>
- Luo Y, Manson AH, Meek CE, Meyer CK, Burrage MD, Fritts DC et al (2002a) The 16-day planetary waves: multi-MF radar observations from the arctic to equator and comparisons with the HRDI measurements and the GSWM modelling results. *Ann Geophys* 20(5):691–709. <https://doi.org/10.5194/angeo-20-691-2002>
- Luo Y, Manson AH, Meek CE, Thayaparan T, MacDougall J, Hocking WK (2002b) The 16-day wave in the mesosphere and lower thermosphere: simultaneous observations at Saskatoon (52°N, 107°W) and London (43°N, 81°W), Canada. *J Atmos Sol Terr Phys* 64:1287–1307. [https://doi.org/10.1016/S1364-6826\(02\)00042-1](https://doi.org/10.1016/S1364-6826(02)00042-1)
- Manney GL, Schwartz MJ, Krüger K, Santee ML, Pawson S, Lee JN et al (2009) Aura Microwave Limb Sounder observations of dynamics and transport during the record-breaking 2009 Arctic stratospheric major warming. *Geophys Res Lett* 36:L12815. <https://doi.org/10.1029/2009GL038586>
- Matsuno T (1971) A dynamical model of the stratospheric sudden warming. *J Atmos Sci* 28(8):1479–1494. [https://doi.org/10.1175/1520-0469\(1971\)028%3c1479:ADMOTS%3e2.0.CO;2](https://doi.org/10.1175/1520-0469(1971)028%3c1479:ADMOTS%3e2.0.CO;2)
- McDonald AJ, Hibbins RE, Jarvis MJ (2011) Properties of the quasi 16 day wave derived from EOS MLS observations. *J Geophys Res Atmos* 116:D06112. <https://doi.org/10.1029/2010JD014719>
- Meek CE, Manson AH (2009) Summer planetary-scale oscillations: aura MLS temperature compared with ground-based radar wind. *Ann Geophys* 27(4):1763–1774. <https://doi.org/10.5194/angeo-27-1763-2009>

- Mitchell NJ, Middleton HR, Beard AG, Williams PJS, Muller HG (1999) The 16-day planetary wave in the mesosphere and lower thermosphere. *Ann Geophys* 17(11):1447–1456. <https://doi.org/10.1007/s00585-999-1447-9>
- Miyoshi Y (1999) Numerical simulation of the 5-day and 16-day waves in the mesopause region. *Earth Planets Space* 51:763–772. <https://doi.org/10.1186/BF03353235>
- Molod A, Takacs L, Suarez M, Bacmeister J (2015) Development of the GEOS-5 atmospheric general circulation model: evolution from MERRA to MERRA2. *Geosci Model Dev* 8:1339–1356. <https://doi.org/10.5194/gmd-8-1339-2015>
- Namboothiri SP, Kishore P, Igarashi K (2002) Climatological studies of the quasi 16-day oscillations in the mesosphere and lower thermosphere at Yamagawa (31.2°N, 130.6°E), Japan. *Ann Geophys* 20(8):1239–1246. <https://doi.org/10.5194/angeo-20-1239-2002>
- Pancheva D, Mukhtarov P, Mitchell NJ, Andonov B, Merzlyakov E, Singer W et al (2008) Latitudinal wave coupling of the stratosphere and mesosphere during the major stratospheric warming in 2003/2004. *Ann Geophys* 26(3):467–483. <https://doi.org/10.5194/angeo-26-467-2008>
- Pancheva D, Mukhtarov P, Andonov B (2009) Nonmigrating tidal activity related to the sudden stratospheric warming in the Arctic winter of 2003/2004. *Ann Geophys* 27(3):975–987. <https://doi.org/10.5194/angeo-27-975-2009>
- Pawson S, Naujokat B (1999) The cold winters of the middle 1990s in the northern lower stratosphere. *J Geophys Res Atmos* 104(D12):14209–14222. <https://doi.org/10.1029/1999JD900211>
- Saha K (2008) The earth's atmosphere. Springer, Berlin
- Salby ML (1981a) Rossby normal modes in nonuniform background configurations. Part I: simple fields. *J Atmos Sci* 38(9):1803–1826. [https://doi.org/10.1175/1520-0469\(1981\)038%3c1803:RNMINB%3e2.0.CO;2](https://doi.org/10.1175/1520-0469(1981)038%3c1803:RNMINB%3e2.0.CO;2)
- Salby ML (1981b) Rossby normal modes in nonuniform background configurations. Part II. Equinox and solstice conditions. *J Atmos Sci* 38(9):1827–1840. [https://doi.org/10.1175/1520-0469\(1981\)038%3c1827:RNMINB%3e2.0.CO;2](https://doi.org/10.1175/1520-0469(1981)038%3c1827:RNMINB%3e2.0.CO;2)
- Salby ML (1984) Survey of planetary-scale traveling waves: The state of theory and observations. *Rev Geophys* 22(2):209–236. <https://doi.org/10.1029/RG022i002p00209>
- Salby ML, Callaghan PF (2001) Seasonal amplification of the 2-day wave: relationship between normal mode and instability. *J Atmos Sci* 58(14):1858–1869. [https://doi.org/10.1175/1520-0469\(2001\)058%3c1858:SAOTDW%3e2.0.CO;2](https://doi.org/10.1175/1520-0469(2001)058%3c1858:SAOTDW%3e2.0.CO;2)
- Shepherd MG, Tsuda T (2008) Large-scale planetary disturbances in stratospheric temperature at high-latitudes in the southern summer hemisphere. *Atmos Chem Phys* 8(24):7557–7570. <https://doi.org/10.5194/acp-8-7557-2008>
- Sox L, Wickwar VB, Fish CS, Herron JP (2016) Connection between the midlatitude mesosphere and sudden stratospheric warmings as measured by Rayleigh-scatter lidar. *J Geophys Res Atmos* 121(9):4627–4636. <https://doi.org/10.1002/2015JD024374>
- Torrence C, Compo GP (1998) A practical guide to wavelet analysis. *Bull Amer Meteor Soc* 79(1):61–78. [https://doi.org/10.1175/1520-0477\(1998\)079%3c0061:APGTWA%3e2.0.CO;2](https://doi.org/10.1175/1520-0477(1998)079%3c0061:APGTWA%3e2.0.CO;2)
- van Oldenborgh GJ, Haarsma R, de Vries H, Allen MR (2015) Cold extremes in North America vs. mild weather in Europe: the winter of 2013–14 in the context of a warming world. *B Am Meteorol Soc* 96(5):707–714. <https://doi.org/10.1175/BAMS-D-14-00036.1>
- Vineeth C, Pant TK, Kumar KK, Ramkumar G, Sridharan R (2009) Signatures of low latitude-high latitude coupling in the tropical MLT region during sudden stratospheric warming. *Geophys Res Lett* 36:L20104. <https://doi.org/10.1029/2009GL040375>
- Wang SY, Hipps L, Gillies RR, Yoon JH (2014) Probable causes of the abnormal ridge accompanying the 2013–2014 California drought: ENSO precursor and anthropogenic warming footprint. *Geophys Res Lett* 41(9):3220–3226. <https://doi.org/10.1002/2014GL059748>
- Wang R, Tomikawa Y, Nakamura T, Huang K, Zhang S, Zhang Y et al (2016) A mechanism to explain the variations of tropopause and tropopause inversion layer in the Arctic region during a sudden stratospheric warming in 2009. *J Geophys Res Atmos* 121(20):11932–11945. <https://doi.org/10.1002/2016JD024958>
- Wehrbein WM, Leovy CB (1982) An accurate radiative heating and cooling algorithm for use in a dynamical model of the middle atmosphere. *J Atmos Sci* 39(7):1532–1544. [https://doi.org/10.1175/1520-0469\(1982\)039%3c1532:AARHAC%3e2.0.CO;2](https://doi.org/10.1175/1520-0469(1982)039%3c1532:AARHAC%3e2.0.CO;2)
- Williams CR, Avery SK (1992) Analysis of long-period waves using the mesosphere-stratosphere-troposphere radar at Poker Flat, Alaska. *J Geophys Res Atmos* 97(D18):20855–20861. <https://doi.org/10.1029/92JD02052>
- Xiong J, Wan W, Ding F, Liu L, Ning B, Niu X (2013) Coupling between mesosphere and ionosphere over Beijing through semidiurnal tides during the 2009 sudden stratospheric warming. *J Geophys Res Space Phys* 118(5):2511–2521. <https://doi.org/10.1002/jgra.50280>
- Yu B, Zhang X (2015) A physical analysis of the severe 2013/2014 cold winter in North America. *J Geophys Res Atmos* 120(19):10149–10165. <https://doi.org/10.1002/2015JD023116>
- Yu Y, Wan W, Ren Z, Xiong B, Zhang Y, Hu L et al (2015) Seasonal variations of MLT tides revealed by a meteor radar chain based on Hough mode decomposition. *J Geophys Res Space Phys* 120(8):7030–7048. <https://doi.org/10.1002/2015JA021276>
- Yu FR, Huang KM, Zhang SD, Huang CM, Yi F, Gong Y et al (2019) Quasi 10- and 16-day wave activities observed through meteor radar and MST radar during stratospheric final warming in 2015 spring. *J Geophys Res Atmos* 124(12):6040–6056. <https://doi.org/10.1029/2019JD030630>
- Yuan T, Thuraiajah B, She CY, Chandran A, Collins RL, Krueger DA (2012) Wind and temperature response of midlatitude mesopause region to the 2009 Sudden Stratospheric Warming. *J Geophys Res* 117:D09114. <https://doi.org/10.1029/2011JD017142>
- Zhang C (2005) Madden-Julian oscillation. *Rev Geophys* 43(2):RG2003. <https://doi.org/10.1029/2004RG000158>

## Publisher's Note

Springer Nature remains neutral with regard to jurisdictional claims in published maps and institutional affiliations.

**Submit your manuscript to a SpringerOpen<sup>®</sup> journal and benefit from:**

- Convenient online submission
- Rigorous peer review
- Open access: articles freely available online
- High visibility within the field
- Retaining the copyright to your article

Submit your next manuscript at ► [springeropen.com](https://www.springeropen.com)